PROCEEDINGS OF SCIENCE

Cosmic ray energy spectrum measurements by Pierre Auger Observatory and Telescope Array

Keitaro Fujita[a,*]

[a] *Institute for Cosmic Ray Research, The University of Tokyo*
5-1-5 Kashiwa-no-Ha, Kashiwa-shi, Chiba, 277-8582, Japan

E-mail: kfujita@icrr.u-tokyo.ac.jp

The measurement of the energy spectrum of cosmic rays is of crucial importance to reveal their origin, propagation, and acceleration mechanisms. The Pierre Auger Observatory in Argentina and the Telescope Array (TA) in the US continue to observe cosmic rays by a hybrid detector, which is composed of Fluorescence Detectors (FD) and Surface Detector (SD) array, in the southern and northern hemispheres respectively. Especially in recent measurements, they successfully measure the cosmic ray spectrum with energies below 10^{16} eV by observing events in which the signals from air showers are dominated by Cherenkov light by high elevation fluorescence telescopes. This contribution reviews the recent measurements by both collaborations, particularly the Cherenkov-based measurements.

**** 27th European Cosmic Ray Symposium - ECRS ****
**** 25-29 July 2022 ****
**** Nijmegen, the Netherlands ****

*Speaker

PoS(ECRS)022

1. Introduction

The origin and nature of cosmic rays is one of the most intriguing unsolved problems in modern astrophysics. Based on previous observations, the probable origins of low energy cosmic rays are supernova remnants and cosmic rays up to 10^{15} eV are believed to be produced and accelerated in our Galaxy. At the energies above about 10^{18} eV, they are believed to be originated in extragalactic sources. However, the origin of cosmic rays still haven't been identified, even more than a century has passed since their discovery. The precise measurement of the cosmic ray energy spectrum is crucial importance to reveal their origin, propagation, and acceleration mechanisms because the absolute scale and its shape are closely related to the production rate in the sources, the spatial distribution of the sources, as well as the cosmic ray propagation. The energy spectrum of comic rays approximately follows power low structure of $\mathrm{d}\Phi/\mathrm{d}E \propto E^{-\gamma}$ in the energy range above 10^{11} eV, where cosmic rays are not affected the solar activity. The index value is changed from $\gamma \sim 2.7$ to $\gamma \sim 3$ at around $10^{15.6}$ eV, commonly known the "knee" feature. At around $\sim 10^{17}$ eV, there is a "2nd knee" structure at which the spectrum steepens to $\gamma \sim 3.2$, then harden again to $\gamma \sim 2.6$ at the "ankle", about $10^{18.7}$ eV, and the steepening to $\gamma \sim 5$ beyond $10^{19.6}$ eV.

For the purpose of unraveling the mystery of ultra-high energy cosmic rays (UHECRs), the Pierre Auger Observatory in Argentina and the Telescope Array (TA) in the United States have been operated more than 10 years. The two observatories have a same strategy as measuring the cosmic ray energy by hybrid design detector that allows calibrating the energy scale of the surface detector (SD) to the fluorescence detector (FD). Furthermore, they extended their observatories to go down to lower energy regions by using the same concept as higher energies. In this contribution, I introduce their detectors, data reconstruction methods, the latest results of both experiments, and recent progress of further extension of their observatories.

2. Observatory

The Pierre Auger Observatory located around 35° S, 69° W near the Mendoza, Argentina, is the largest cosmic ray observatory in the world. Its layout is shown in the left panel of Fig. 1. The surface detectors array consists of 1600 water Cherenkov detector deployed in triangle grid with 1500 m spacing (SD1500) and covers about 3000 km^2 area in total. Each water tank have cylindrical shape with 1.8 m radius, 1.2 m depth, and contains $\sim$ 12000 L of highly purified water. On top of the tank, three photomultipliers are mounted, pointing downward in the water, and collect light that is proportional to the energy of $\gamma/e^{\pm}$ and track length of $\mu^{\pm}$ in the tank. The four fluorescence detector stations, which consist of six fluorescence telescopes with elevation angle from 1° to 30°, with 30° in azimuthal angle, are looking the atmosphere over the area of SD array. Each fluorescence telescope is composed of a segmented spherical mirror of 10 m^2 and a camera of 440 hexagonal surface photomultipliers, which pixel is about 1.5° × 1.5°. A photograph of one of the SDs and FD station are shown in the right panel of Fig. 1. In the North-Western part of the observatory, the three high elevation telescopes (HEAT) with elevation from 30° to 60° and a 750 m spacing denser array with 61 water Cherenkov detector (SD750), which total coverage is approximately 24 km^2, are deployed to explore low energy cosmic rays with energies above $\sim 10^{16}$ eV. Detail descriptions can be found in [1].

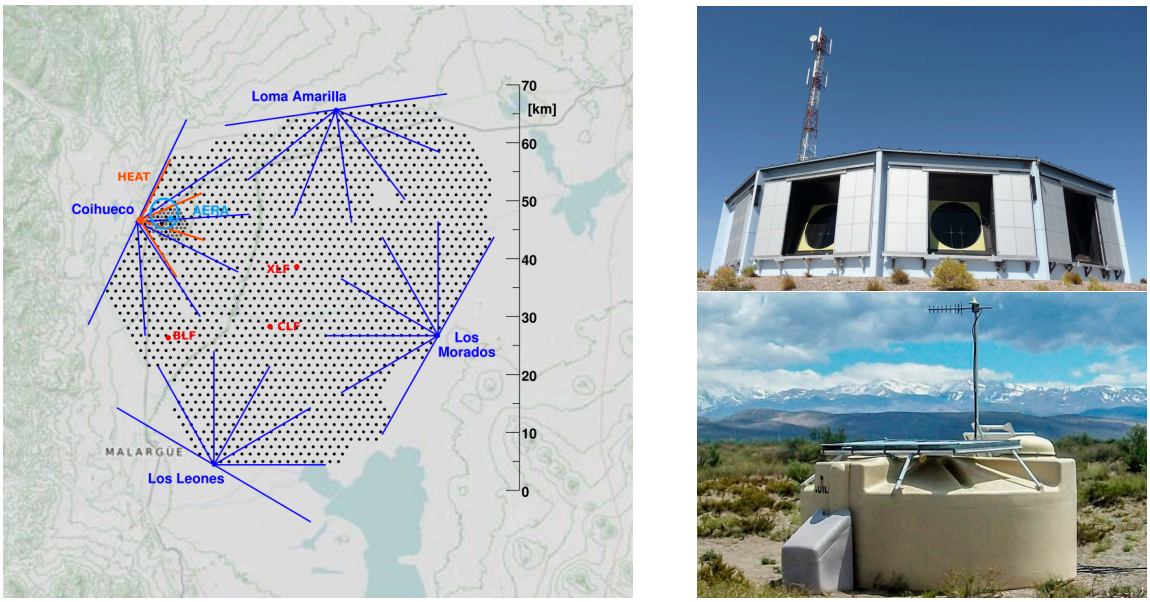

Figure 1: *Left*: The Pierre Auger Observatory layout. Each dot corresponds to one of the 1600 surface detector stations. The four fluorescence detector sites are shown, each with the field of view of its six telescopes. The Coihueco site hosts three extra high elevation (HEAT) telescopes. The 750 m array is located a few kilometers from Coihueco [2]. *Right – Top*: FD building at Los Leones site [1]. *Right – Bottom*: One of the SD stations in the Auger site. [2].

The Telescope Array located around 39° S, 113° W has the largest cosmic ray observatory in the northern hemisphere. The main part of the experiment consists of a SD array and three FD stations that are viewing over the SD area. The TA SD deployed 507 scintillation counters in square grid with 1200 m spacing and covering a total of $\sim$ 700 km^2 area on the ground. Each surface counter has two layers of a 3 m^2 plastic scintillator with 1.2 cm thickness. The scintillation lights produced by the charged particles energy deposition are led to the photomultipliers that connected from each layer through wavelength shifting fibers. The three TA FD stations are located at Black Rock Mesa (BRM), Long Ridge (LR), and Middle Drum (MD) with viewing from 3° to 31° in elevation. The fluorescence telescope of TA are composed of segmented spherical mirror and and a camera of 256 hexagonal surface photomultipliers, which field of view is 1° $\times$ 1°. The Telescope Array Low-energy Extension (TALE), located at the north part of the TA Experiment site, is aimed at measuring the low energy cosmic rays above 10^{16} eV. The TALE detector consists of one FD station with ten fluorescence telescopes, which viewing a high elevation angle of 31° - 59° directly above the field of view of the MD telescopes (field of views are shown by blue points in the top-left in Fig. 2), and an array of 80 scintillation surface detectors, which were deployed to cover a total area of approximately 20 km^2. A photo of one of the SDs and FD station are shown in the right panel of Fig. 2. Detail descriptions can be found in [3–5].

3. Energy measurements

3.1 Hybrid approach

The hybrid design system has advantages for studying cosmic rays: the FD measurement is able to observe the longitudinal shower development directly and measure the cosmic ray energy without

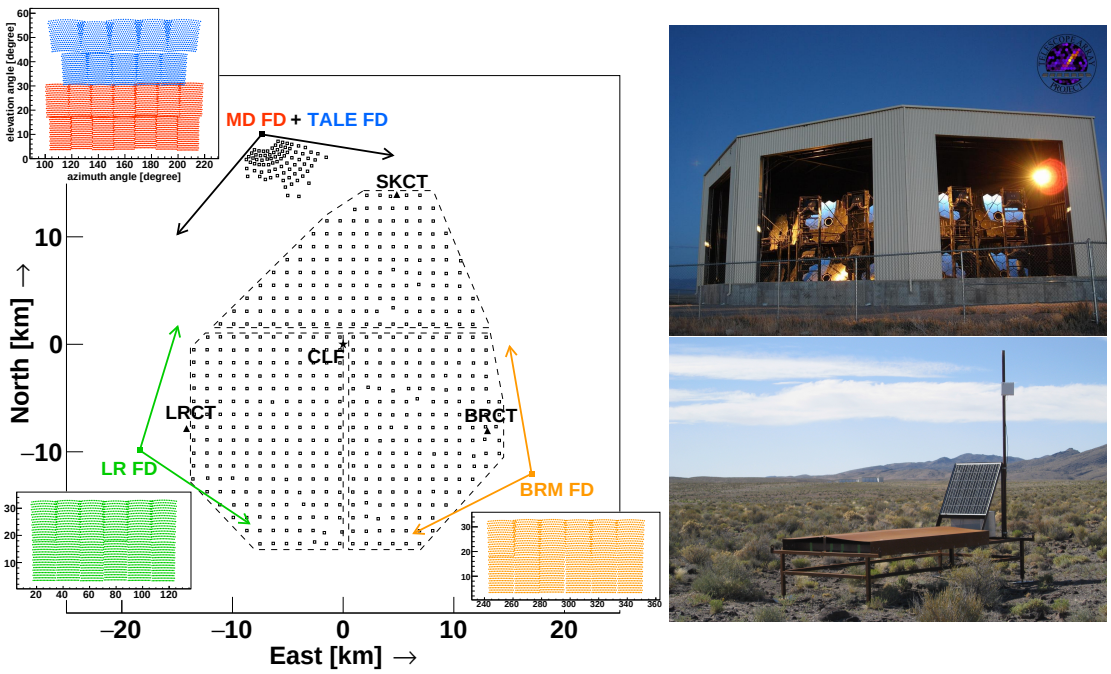

Figure 2: *Left*: The Telescope Array layout. Each TA SD location is indicated by white squares. Each FD location are represented by filled square. The arrows originated from each FD station are represented the edge of FD field of view. In addition, each FD filed of view is plotted beside of the location of FD with same color. Northwest array, which is near from MD station, is the TALE SD array. *Right – Top*: FD building at Black Rock Mesa site. *Right – Bottom*: One of the SD in the TA site.

hadronic interaction model dependence, and the SD measurement is still only useful method that has a 100 % duty cycle. In addition, hybrid observation, where the same event is detected by both FD and SDs, can combine some of the advantages of both. In particular, the hybrid observation improves the shower geometry accuracy compared with the event only seen by FD or SD because the time information from the SD constrains the arrival time and impact point of the shower at the ground. Eventually, the hybrid events provide the most accurate energy resolution. In fact, Auger and TA achieve 8 % energy resolution in hybrid mode.

3.2 Energy estimation from surface detector data

The SD reconstruction is based on three processes; the geometry fit, the lateral distribution function (LDF) fit, and the energy estimation. The geometry fit and LDF fit have done by using the time information and total signal in the VEM unit of triggered SDs that comes from the combination of their total waveforms. For both SD arrays, the signal that would be detected by a station located at a reference distance from the shower axis is used as the cosmic ray energy estimator. The reference distance, 1000 m for Auger SD1500 array and 800 m for TA SD array, is chosen to minimize the fluctuations of the shower signal. The differences in reference distances depend on the detector type and the detector spacing.

The energy estimator $S(1000)$ for the Auger SD1500 array is converted into S_{38}, the particle density that would have been observed a shower arrived at $\theta = 38°$, by means of the constant intensity cut (CIC) method [6] that taking into account the atmospheric attenuation for different

zenith angles of cosmic ray arrival directions. The corrected shower size is subsequently calibrated against the FD energies using a power-law function, $E = AS_{38}^{B}$ (Fig. 3). The statistical uncertainty in the energy scale arising from the fit of the two calibration parameters is below 1%.

For the TA SD case, the energy estimation table is constructed by using large statistic Monte-Carlo simulations of showers (Fig. 4). The obtained energies from lookup table are calibrated against the FD energies using events that are seen in common by both TA SD and FD and are well reconstructed by each detector separately. In order to match the TA FD energy, the TA SD energies determined from the energy estimation table need to be reduced by a factor 1/1.27. TA also established the CIC-based energy determination: for TA the energies calculated by the two methods agree within 3% [7].

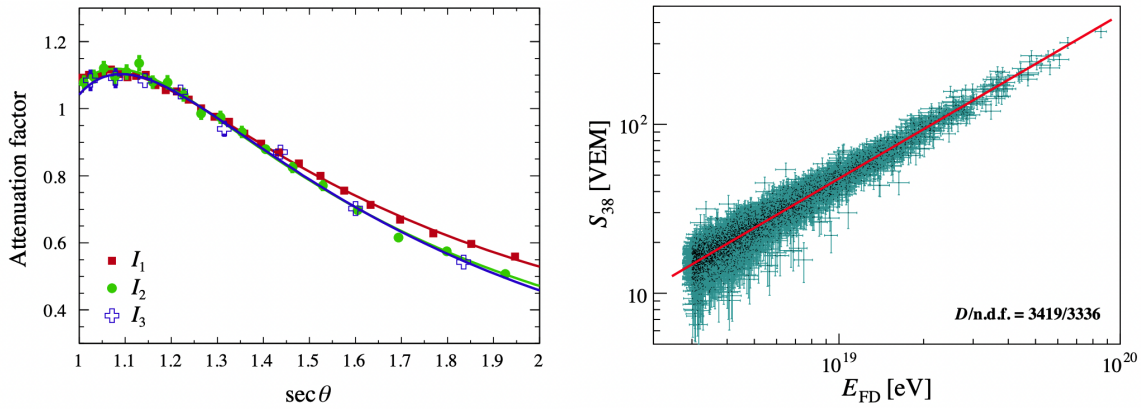

Figure 3: *Left*: $S(1000)$ attenuation, normalized to 1 at $\theta = 38°$, as a function of sec θ, as derived from the CIC method, for different intensity thresholds. *Right*: Correlation between the SD energy estimator, S_{38}, and the reconstructed FD energy, E_{FD}, for the selected 3,338 hybrid events is plotted. The solid line is the best fit of the power-law dependence $E_{FD} = AS_{38}^{B}$ to the data [6].

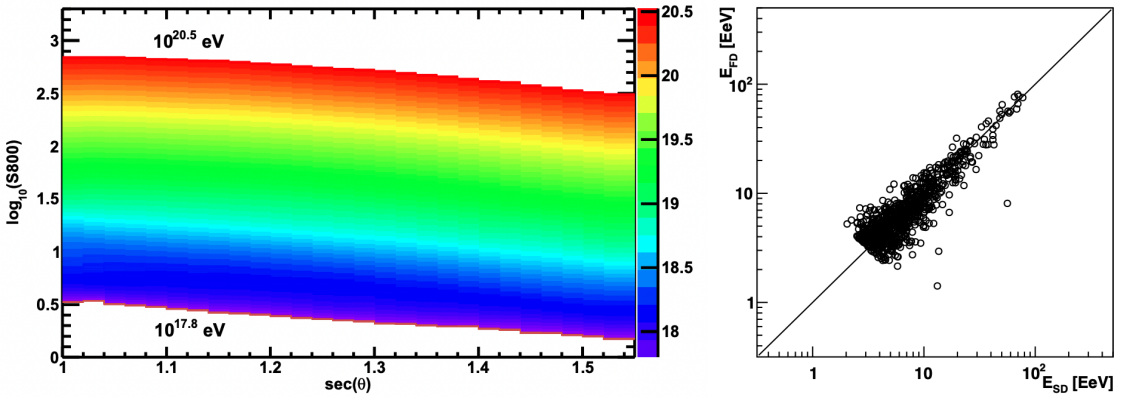

Figure 4: *Left*: The first energy estimation table for TA SD events as functions of reconstructed $S(800)$ and secθ. The table made from the MC which shares all characteristics of the real data and has been processed by the same reconstruction prosecces as the real data [8]. *Right*: TA FD and TA SD energy comparison plots using 8.5 years well reconstructed hybrid event by both mode. The TA SD MC-driven energy has been scale by 1/1.27 before making these comparison. The solid line represents the $E_{SD} = E_{FD}$ case.

3.3 Low energy cosmic rays seen by Cherenkov light

In the energy range of roughly less than 10^{17} eV, Auger and TA use the HEAT and TALE-FD as an Imaging Air Cerenkov Telescope (IACT) to extend the energy threshold of the detector down $\sim 10^{15}$ eV. The Cherenkov light produced by a shower has a same characteristic as fluorescence light that both are directly proportional to the number of shower particles for any given point in the shower development. This property means that the observed Cherenkov signal can be used to infer the shower properties (energy and $X_{\rm max}$) in a similar way to how the fluorescence light is used. A significant difference between the Cherenkov and fluorescence light is that the Cherenkov light emitted by the shower particles is strongly peaked forward along the shower direction, and falls off rapidly as the shower viewing angle changes while the fluorescence light is emitted isotropically. As a result, Cherenkov events are seen only if the shower geometry with respect to the detector is such that the shower is moving towards the detector (viewing angle $\sim 10^\circ$ or smaller), and are observed much faster (total event duration and shower image are much shorter) than fluorescence dominated events seen by hybrid detector energies above 10^{18} eV. Due to the above reasons, the lower energy events seen by Cherenkov light are processed reconstruction by the Profile-Constrained Geometry Fit (PCGF) that simultaneously reconstructs the shower geometry and the shower profile, originally developed by the HiRes collaboration [9]. This method scans over all possible shower geometries compatible with the arrival times of photons at individual pixels of the FD camera and for each such geometry calculates a trial shower profile in the atmosphere. The best expectation of the shower geometry and energy deposit profile from a cosmic ray shower is chosen. Auger and TA achieve 1° angular resolution and 10 % energy resolution at 10^{16} eV.

4. The ultra-high energy cosmic rays energy spectrum

The comparison of whole sky spectra measured by Auger and TA is presented in the left panel of Fig. 5. The systematic difference in the absolute energy scale between both measurements is at a level of $\sim 9\%$. A first difference comes from the fluorescence yield, which is the number of fluorescence photons emitted by atmospheric molecules per unit energy deposited by the charged particles. The absolute fluorescence yield measured by the AirFly experiment [10] is used at the Auger Observatory, while the combination of the absolute fluorescence yield measured by Kakimoto et al. [11] and the fluorescence line spectrum measured by the FLASH experiment [12] is used in the TA measurement. Note that TA energies would decrease by 14% after synchronizing the fluorescence yield to that used at the Auger Observatory [13]. A second difference is in an invisible energy correction. Some portion of the shower energies are carried by low-energy muons and neutral particles, mainly neutrinos and neutrons, because they do not deposit all their energy in the atmosphere, i.e., the fluorescence and Cherenkov light are not emitted via these particles. Therefore, it is required to correct the measured calorimetric energy to obtain the primary energy of the cosmic ray. In TA case, the invisible energy correction is evaluated from simulated proton-induced showers [14]. On the other hand, in Auger case, the invisible energies are estimated by their observable parameters using hybrid events [15]. The energy scale difference comes from invisible energy correction is ~ 7 % on the opposite side of the fluorescence yield difference [13]. The value of 9% level difference on the energy scale is well understood within the systematic uncertainty as

discussed above. The energy spectra after rescaling the energies by + 4.5 % for Auger and -4.5 % for TA better agree as shown in the right panel of Fig. 5.

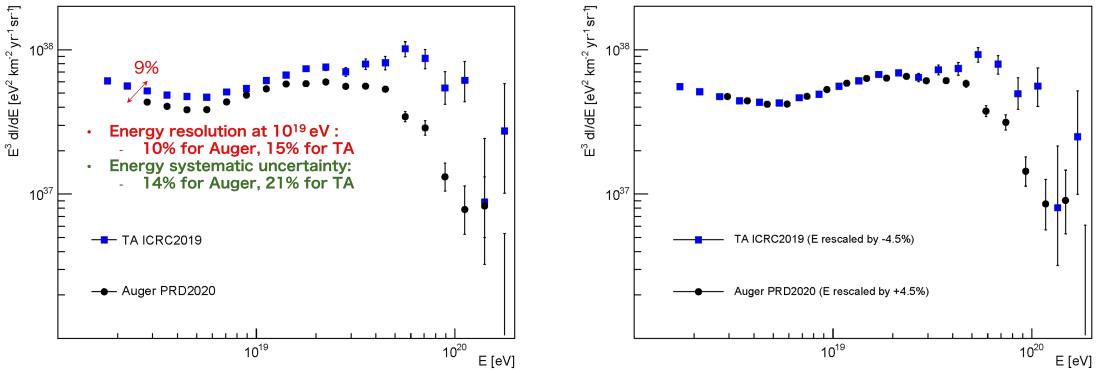

Figure 5: *Left*: Auger SD1500 and TA SD energy spectra in the full fields of view (-90° < δ < +24.8° and 15.7° < δ < +90° respectively) [6, 16]. *Right*: Energy rescaled spectra by ± 4.5% in opposite side.

4.1 Comparison in common declination band spectrum

The energy spectra after rescaling ± 4.5 % in the common declination band that can be seen by both observatories (-15.7° < δ < +24.8°) are presented in the left panel of Fig. 6. The energy spectrum difference in the highest region is smaller than whole sky spectra. However, an additional energy dependence rescaling in the energies above 10^{19} eV (± 10 % / decade) is required to get an even better agreement (right panel of Fig. 6).

the Auger spectra divided by three declination bands of equal exposure, shown in the left panel of Fig. 7, clearly shows that there is no strong dependence of the fluxes on declination, while the TA spectra in a lower and higher declination band shows slightly different cutoff energies as shown in the right panel of Fig. 7. The global significance of this declination dependence effect is estimated to be 4.3 σ [16]. No systematic and instrumental effects have been identified to explain the additional ± 10 % energy dependence shift and the declination dependence in the spectrum.

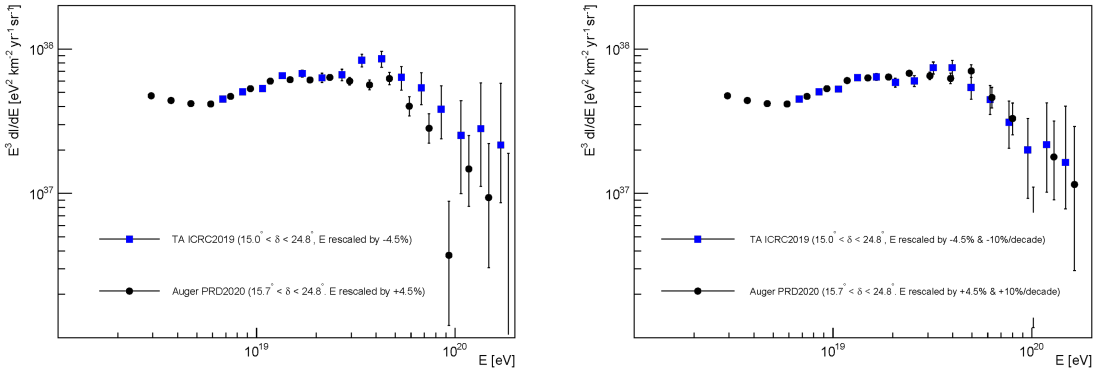

Figure 6: *Left*: Auger SD1500 and TA SD spectra in the common declination band (-15.7° < δ < +24.8°) with a constant energy shift of ± 4.5 %. *Right*: Auger and TA spectra in the common declination band with ± 4.5 % energy shift and ± 10 % energy dependence shift in energies above $10^{19.0}$ eV [13].

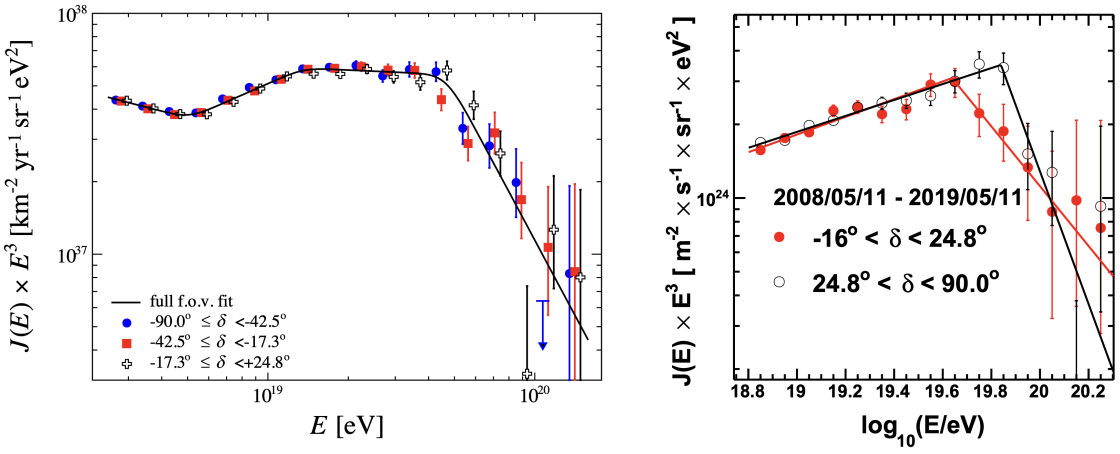

Figure 7: *Left*: Auger SD1500 energy spectra in three declination bands of equal exposure [6]. The best fit of the whole sky spectrum is shown as the black line. *Right*: TA SD energy spectra for the upper and lower declination bands. Superimposed are the fits to the broken power law functions [16].

4.2 New feature in the energy spectrum

A new feature, which calls here the *instep*, was initially observed by the Auger collaboration in 2020 [17]. The Auger field of view is concentrated mostly in the southern hemisphere. They have reported that there are two break features above the ankle. The ankle energy is described at $E = 10^{18.70}$ eV, with a hardening spectrum from $\gamma_1 = -3.29$ to $\gamma_2 = -2.51$. At the instep, $E = 10^{19.11}$ eV, the spectrum softens from $\gamma_2 = -2.51$ to $\gamma_3 = -3.05$. Finally, the spectrum softens above suppression energy, at $E = 10^{19.66}$ eV, with $\gamma_4 = -5.1$.

The new feature of two-step softening of the spectrum has also been tested in the northern hemisphere measurements by using HiRes and TA data. TA performed a joint fit of TA SD, TA BRM + LR FD monocular, and HiRes I monocular spectra into three times broken power-law. The TA FD monocular observation period was removed from the TA SD spectrum measurement to ensure statistical independence. The instep feature was confirmed as shown in Fig. 8. In the northern hemisphere measurements, the ankle is located at $E = 10^{18.73}$ eV, with spectrum hardening from $\gamma_1 = -3.23$ to $\gamma_2 = -2.62$. The spectrum softens from $\gamma_2 = -2.62$ to $\gamma_3 = -2.92$ at the instep, $E = 10^{19.25}$ eV. Finally, the spectrum is suppressed at $E = 10^{19.85}$ eV, with $\gamma_4 = -5.0$. The number of expected events between $10^{19.25}$ and $10^{19.85}$ eV is 1269 if the instep feature is absent, while the number of events actually measured by HiRes and TA in that energy range is 1086. Thus, an assumption of no breaks before the high-energy suppression is rejected with 5.3σ confidence.

5. Low energy spectrum

5.1 SD measurement

Auger extends their spectrum measurements down to lower energies by using the Auger SD750 array. The energy determination for the Auger SD750 measurement is similar to the one performed with the 1500 m array. The expected signal at 450 m far from the axis, $S(450)$, has been used to estimate the shower energy. As same as the 1500 m array, the energy estimator $S(450)$ is converted

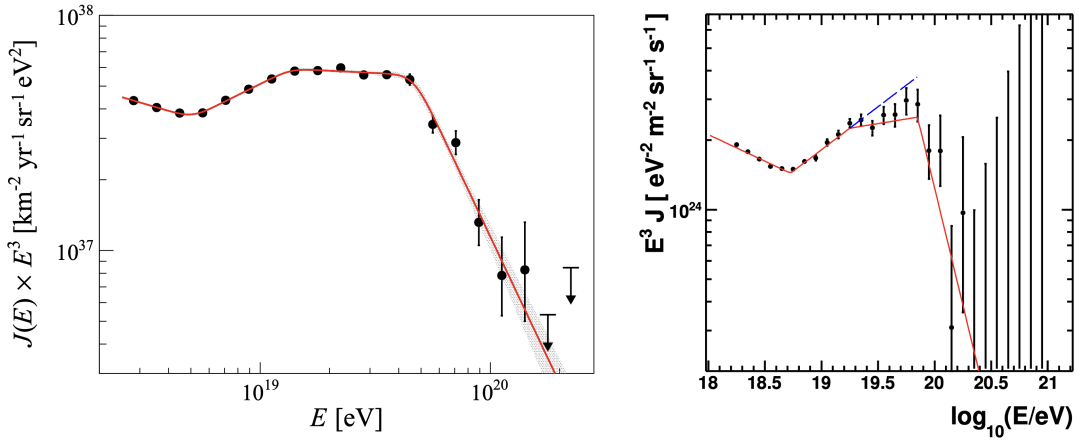

Figure 8: *Left*: The Auger energy spectrum fitted with four power-laws [17]. *Right*: The TA SD energy spectrum together with the joint fit with three break points in red. The significance of the instep is obtained by comparing the number of events expected in the absence of the feature (blue line) and the number of events by the experiments [18].

into S_{35} by the CIC method, and finally scaled to the FD energies [19]. The energy spectrum as measured by the Auger SD750 array is shown in the left panel of Fig. 9.

5.2 Cherenkov measurements

As discussed in Sec. 3.3, the lower energy measurements by the FDs are based on the detection of the Cherenkov light emitted from the air shower. A detailed simulation of air showers, light emission in the atmosphere, and the detector status are needed to calculate the detector aperture accurately. The results of spectrum measurement in lower energy by the HEAT telescopes and the TALE detector are shown in Fig. 9, 10. As we see, it is clearly observed the *low-energy ankle* above 10^{16} eV, and the 2*nd knee* at 10^{17} eV.

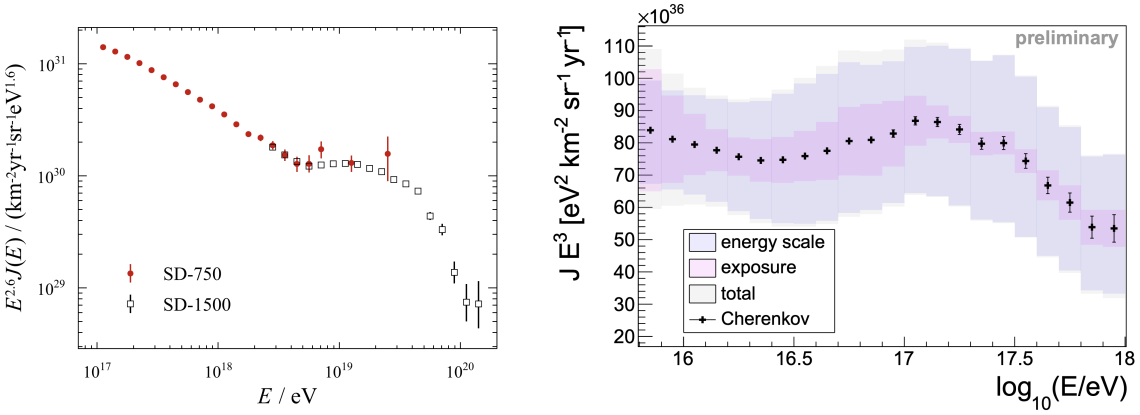

Figure 9: *Left*: Auger SD spectra measured with the SD750 (red circles) and the SD1500 (black squares) data [19]. *Right*: Energy spectrum measured by HEAT telescopes. The systematic uncertainty related to exposure is shown by the magenta band, that corresponding to the energy scale by the blue band, and the total systematic uncertainty by the gray band [20].

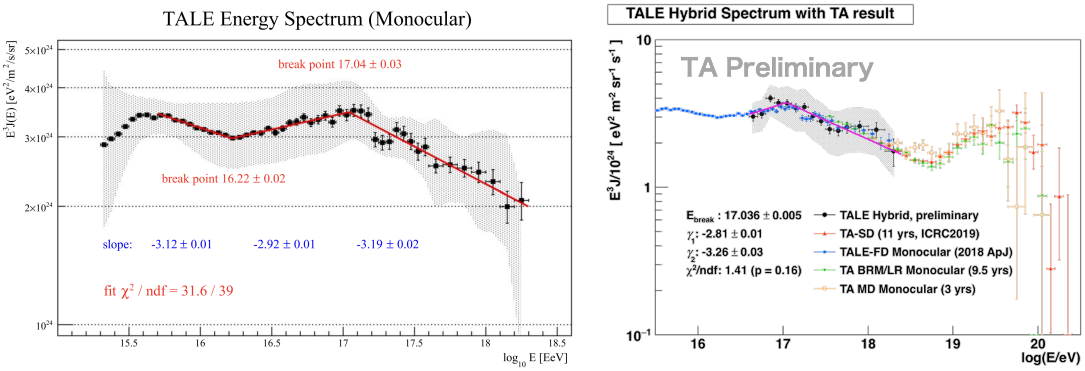

Figure 10: *Left*: TALE-FD monocular energy spectrum measured with 22 months of data [21]. The gray band indicates the size of the systematic uncertainties. *Right*: TALE-Hybrid energy spectrum measured with almost 2 years of data is shown by the black points. The gray band indicates the size of the systematic uncertainties, and the best fit broken power-low function is drowned by the magenta line. The others are previous TA measurements using TA FD [21–23] and TA SD data [16].

6. Conclusion

It has been reviewed the present status of measurements of the cosmic ray energy spectrum with energies from PeV range to the highest energies by the Pierre Auger Observatory and the Telescope Array. The spectra measured by both experiments are basically in agreement in the energy range of $E < 10^{19}$ eV within the systematic uncertainties of the energy scale.

Both Auger and TA, are upgrading their detectors. These are the so-called AugerPrime and TA×4. The AugerPrime installs a scintillation counter to measure the electromagnetic components of the air shower for the vertical events, a radio antenna to measure the same ones for the inclined showers, and small PMT for the wider dynamic range, to the existing water Cherenkov tanks, to enhance the mass-discrimination power. TA×4 quadruples the effective area of the original TA SD array installing additional 250 scintillation counters in the northern and southern areas of the main array. In addition to the SD array, in total 12 telescopes were constructed to increase the statistics of the hybrid event for the clarification of the cosmic ray composition in the highest energies. Further data analysis with increased statistics and composition measurements will permit disentangling the differences in the two experiments and interpretation both in technical and astrophysical aspects.

References

[1] **Pierre Auger** collaboration, A. Aab et al., *Nucl. Instrum. Meth. A* **798** (2015) 172 [1502.01323].

[2] **Pierre Auger** collaboration, A. Aab et al., 1604.03637.

[3] **Telescope Array** collaboration, H. Tokuno et al., *Nucl. Instrum. Meth. A* **676** (2012) 54 [1201.0002].

[4] **Telescope Array** collaboration, T. Abu-Zayyad, R. Aida, M. Allen, R. Anderson, R. Azuma, E. Barcikowski et al., *Nucl. Instrum. Meth. A* **689** (2012) 87.

[5] **Telescope Array** collaboration, S. Ogio, *PoS* **ICRC2019** (2019) 375.

[6] **Pierre Auger** collaboration, A. Aab, P. Abreu, M. Aglietta, J.M. Albury, I. Allekotte, A. Almela et al., *Phys. Rev. D* **102** (2020) 062005.

[7] **Telescope Array** collaboration, D.Ivanov, *EPJ Web Conf.* **210** (2019) 01001.

[8] **Telescope Array** collaboration, in *33rd International Cosmic Ray Conference*, p. 0395, 2013.

[9] **HiRes** collaboration, R.U. Abbasi et al., *Phys. Rev. Lett.* **100** (2008) 101101 [astro-ph/0703099].

[10] **AIRFLY** collaboration, M. Ave et al., *Astropart. Phys.* **42** (2013) 90 [1210.6734].

[11] F. Kakimoto, E.C. Loh, M. Nagano, H. Okuno, M. Teshima and S. Ueno, *Nucl. Instrum. Meth. A* **372** (1996) 527.

[12] R. Abbasi et al., *Astropart. Phys.* **29** (2008) 77 [0708.3116].

[13] **Telescope Array, Pierre Auger** collaboration, R. Abbasi et al., *PoS* **ICRC2021** (2021) 337.

[14] **Telescope Array** collaboration, R.U. Abbasi et al., *Astrophys. J.* **858** (2018) 76 [1801.09784].

[15] **Pierre Auger** collaboration, A. Aab et al., *Phys. Rev. D* **100** (2019) 082003 [1901.08040].

[16] **Telescope Array** collaboration, D.Ivanov, *PoS* **ICRC2019** (2020) 298.

[17] **Pierre Auger** collaboration, A. Aab, P. Abreu, M. Aglietta, J.M. Albury, I. Allekotte, A. Almela et al., *Phys. Rev. Lett.* **125** (2020) 121106.

[18] **Telescope Array** collaboration, D. Ivanov, D. Bergman, G. Furlich, R. Gonzalez, G. Thomson and Y. Tsunesada, *PoS* **ICRC2021** (2021) 341.

[19] **Pierre Auger** collaboration, P. Abreu et al., *Eur. Phys. J. C* **81** (2021) 966 [2109.13400].

[20] V. Novotný, P. Abreu, M. Aglietta, J.M. Albury, I. Allekotte, A. Almela et al., *PoS* **ICRC2021** (2021) 324.

[21] **Telescope Array** collaboration, R.U. Abbasi et al., *Astrophys. J.* **865** (2018) 74 [1803.01288].

[22] **Telescope Array** collaboration, R.U. Abbasi et al., *Astropart. Phys.* **80** (2016) 131 [1511.07510].

[23] **Telescope Array** collaboration, T. Abu-Zayyad et al., *Astropart. Phys.* **39-40** (2012) 109 [1202.5141].